Observation of GHG vertical profile in the boundary layer of the Mount Qomolangma region using a multirotor UAV

Ying Zhou[1,2], Congcong Qiao[1,2], Minqiang Zhou[1,2], Yilong Wang[2,3], Xiangjun Tian[2,3], Yinghong Wang[4], and Minzheng Duan[1,2]

[1]Key Laboratory of Middle Atmosphere and Global Environment Observation, Institute of Atmospheric Physics, Chinese Academy of Sciences, Beijing 10029, China
[2]University of Chinese Academy of Sciences, Beijing 100049, China
[3]State Key Laboratory of Tibetan Plateau Earth System, Environment and Resources, Institute of Tibetan Plateau Research, Chinese Academy of Sciences, Beijing 100101, China
[4]Public Technology Center, Institute of Atmospheric Physics, Chinese Academy of Sciences, Beijing 10029, China

Correspondence: Yilong Wang (wangyilong@itpcas.ac.cn) and Minzheng Duan (dmz@mail.iap.ac.cn)

Abstract. Understanding the vertical profile of greenhouse gases (GHGs) is crucial for elucidating their sources and sinks, transport pathways, and influence on Earth's radiative balance, as well as for enhancing predictive capabilities for climate change. Remote sensing methods for measuring vertical GHG profiles often involve substantial uncertainties, while in-situ measurements are limited by high equipment costs and operational expenses, rendering them impractical for long-term continuous observation efforts. In this study, we have developed an automatic low-cost and user-friendly multi-altitude atmospheric sampling device designed for small and medium-sized unmanned aerial vehicles (UAVs), balloons, and other flight platforms. A field campaign was carried out in the Mount Qomolangma region, at an average surface altitude of 4300 m above sea level (a.s.l.). ~~In total~~During the campaign, we conducted 15 flights ~~with~~ and collected 139 samples from the ground surface up to a height of 1215 m using ~~the device mounted on~~ a hexacopter UAV platform equipped with the sampling device. The samples were analyzed using the Agilent gas chromatography (GC) 7890A, ~~and the vertical profiles of~~ enabling the derivation of the vertical profiles for four GHG species (CO_2, CH_4, N_2O, and SF_6) ~~were archived. The new data depict the vertical distribution of GHGs in the~~ within the boundary layer of the Mount Qomolangma region. To ~~apply this method for~~ enable the long-term monitoring ~~of~~ using small UAVs, future efforts ~~must focus on~~ should prioritize reducing the weight of the equipment and improving the sampling efficiency.

1 Introduction

Contemporary global warming, ~~primarily~~ predominantly driven by human activities, is an urgent environmental challenge ~~marked by an~~ characterized by a significant increase in the atmospheric concentration of greenhouse gases (GHGs), causing a rapid rise in global temperature since the Industrial Revolution(Masson-Delmotte et al., 2019; Friedlingstein et al., 2023). Monitoring the changes in GHG concentration is essential for understanding climate change and promoting environmental protection. Carbon dioxide (CO_2) is the most ~~potent GHG, whose radiative forcing has reached $1.82 \pm 0.19 \mathrm{W/m^2}$ from 1750 to~~ influential GHG, with its radiative forcing reaching $+1.82 \pm 0.19 \mathrm{W/m^2}$ in 2019 ~~(?)~~relative to 1750 (IPCC, 2021), followed

by methane (CH_4), nitrous oxide (N_2O) and other GHGs. The concentrations of GHGs are influenced by surface fluxes and atmospheric chemical transport, leading to ~~spatial distributions that are not uniform. Variations in emissions from natural and anthropogenic sources and atmospheric circulation patterns resultin significant differences in greenhouse gas concentrations at different altitudes(Carnell and Senior, 1998; Ren et al., 2011; Xie et al., 2013).~~

~~Vertical distribution of these GHGs is useful to elucidate their sources and sinks, as well as the vertical mixing of the atmosphere.~~ non-uniform spatial distributions. As a result, measurements of the spatio-temporal distribution of GHG concentrations can be used to derive the sizes of fluxes and the impacts of atmospheric transports. (Carnell and Senior, 1998; Ren et al., 2011; Xie et al., 20 . For instance, the vertical profiles of CO_2 observed by aircraft were used for diagnosing errors in the simulation of surface CO_2 fluxes (Jin et al., 2024) and have been integrated into inverse modeling of carbon fluxes (Niwa et al., 2012; Jiang et al., 2013). ~~It has been shown that satellite-based CO_2 inversions can yield results comparable to surface network inversions when supplemented with aircraft observations to reduce errors(Chevallier et al., 2019). Furthermore, combining surface-based and space-based CO_2 measurements within a flux inversion framework improves constraints on regional CO_2 fluxes compared to using either data source alone(Byrne et al., 2020).~~ Additionally, the vertical distribution of GHGs ~~provides key prior values~~ serves as a critical input for satellite remote sensing retrieval algorithms, enhancing the accuracy of satellite retrievals (Ramanathan et al., 2018; Bao et al., 2020). ~~The Global Carbon Project (GCP) also recommends this type of data (Friedlingstein et al., 2022)~~ This accuracy is critical for atmospheric inversions, whether assimilating satellite data independently (Chevallier et al., 2019) or in conjunction with surface-based measurements (Byrne et al., 2020).

There are two primary methods for obtaining the vertical distribution of atmospheric GHGs: indirect measurements (remote sensing technique) and direct measurements. The first approach involves analyzing the observed characteristic spectrum through space-based satellites or payloads (Buchwitz et al., 2005; O'Dell et al., 2012; Yoshida et al., 2013), ground-based Lidar (Kuma et al., 2021), and high-resolution spectrometers (Wunch et al., 2011). The accuracy of indirect measurement methods ~~for quantifying GHG sources and sinks~~ is limited by several factors, such as cloud cover, aerosols, and surface reflections. These limitations lead to considerable uncertainty and limited spatial resolution of GHG ~~data, as well as challenges in detecting localized changes in~~ concentrations, thereby affecting the accuracy of estimation of localized GHG sources and sinks.

The direct measurement technique requires the use of specialized equipment capable of accurately measuring the atmosphere's composition, such as the devices using the Cavity Ring-down Spectroscopy (CRDS) technique (Wheeler et al., 1998; Wilkinson et al., 2018). To acquire vertical distribution information, multiple inlets are often installed at different altitudes of a tower, which typically only extends a few hundred meters (Haszpra et al., 2012). Alternatively, ~~measurements can be carried aloft by planes~~ lightweight measurement devices can be deployed on aircraft (Sun et al., 2020) or balloons ~~(Li et al., 2014; Bao et al., 2020), although these methods come with significant logistical, cost, and airspace limitations.~~ (Li et al., 2014; Ba to enable in-situ measurements at high altitudes. Sampling devices may also be employed to collect high-altitude air masses for subsequent laboratory analysis. Compared to remote sensing, direct measurements provide higher precision and vertical resolution for GHG data that can be easily tied to ~~the calibration standards~~ calibration standards (e.g. the National Institute of Standards and Technology, NIST scale). Recently, advancements in Unmanned Aerial Vehicles (UAVs) have provided a

lightweight, easy-to-operate, and easily recoverable platform for vertical observations. Due to their small size, portability, and low cost, UAVs have emerged as a popular method for obtaining the distribution of atmospheric constituents, effectively overcoming the limitations of traditional methods (Glaser et al., 2003; Neumann and Bartholmai, 2015; Etts et al., 2015; Brosy et al., 2017; Chang et al., 2020).

Many works have used UAVs for in-situ ~~observation~~ measurements of GHGs, primarily utilizing Non-Dispersive Infrared (NDIR) sensors to measure CO_2 and CH_4 (Kunz et al., 2018; Reuter et al., 2021; Britto Hupsel de Azevedo et al., 2022; Han et al., 2024). While NDIR and other low-cost sensors have the advantage of real-time and continuous monitoring due to their lightweight design, they face challenges such as ~~frequent calibration and potential fluctuation due to the change of~~ the need for frequent calibration arising from fluctuations in ambient environments such as pressure, temperature and ~~also vapor contentin the variable atmosphere along with altitude~~ water vapor content, which vary across locations and altitudes (Liu et al., 2022). In contrast, flask(usually made of metal) ~~analysis allows air samples to be collected and analyzed in a controlled laboratory~~ sampling methods enable the collection and subsequent laboratory analysis under controlled conditions (Loftfield et al., 1997), but they require labor-intensive flask evacuation and cleaning ~~is more labor-intensive, and it is not easy to operate in-flight~~ procedures and are unsuitable for real-time measurements. We have developed a device similar to flask sampling but ~~aluminum bags are used~~using aluminum bags, featuring a lighter design, and expanded its capabilities to analyze additional GHG components. Note that our system requires a higher payload capacity and a larger platform size than ~~online~~ real-time analysis sensors. This portable device operates automatically and can collect air samples from multiple altitudes in a short period. Comprehensive indoor tests verified the device's sampling speed and liability for field measurements. The device was used in a five-day campaign of field measurements on Mount Cho Oyu Basecamp (4950 m a.s.l.) and Mount Qomolangma Station (4300 m a.s.l) between 29 September and 03 October 2023. The device was taken by a medium-sized UAV up to 1250 meters above the ground. During the flights, air samples were collected at different altitudes form the ground to the upper air. The samples were then analysed by a chromatography to derive gas concentrations, including CO_2, CH_4, N_2O, and SF_6.

The paper is structured as follows: Section 2 provides an overview of the gas collection system, and outlines the sampling and analysis procedures used in this experiment. Section 3 details the field experiments, including site descriptions and a discussion of the results. Finally, Section 4 summarizes the key findings and their implications.

2 Methodology

2.1 Gas collection system

The schematic of the automatic sampling device is shown in Figure 1. Airbags are used to collect air samples. Each airbag is a vacuum-sealed, 1 L aluminum-foil bag, sized appropriately for GC analysis. Ten airbags (~~for simplicity, only four bags are illustrated) each feature~~ illustrated here with four for simplicity) are each equipped with a self-sealing structured polycarbonate (PC) stopcock straight valve and ~~are~~ connected to ten micro vacuum pumps ~~via~~ through airtight tubing well-sealed tubes~~. Each pump has~~ , with each pump having an inlet and an outlet. A Hydrophobic (PTFE) filter with a 0.45 μm pore size is attached to the inlet ~~for prohibiting the dust~~ to prevent dust contamination. The outlet is tightly connected to the valve of the sampling

bag, allowing collecting air when the valve is opened. All airbags are stored in a storage box to ensure the safety in case of strong wind. A GPS-receiver and a meteorological sensor (iMET XQ2~~) are used. iMET XQ2 is the second-generation sensor manufactured by~~ , International Met Systems~~, it is designed for UAV deployment, with a 5-hour rechargeable lithium battery and 15-hour data storage. It operates within a relative humidity range of 0-100 %, a temperaturerange of~~) form an integrated data acquisition system capable of simultaneously recording time and position (longitude, latitude, altitude), and atmospheric parameters (pressure: 10-1200 hPa; temperature: -90°C to +50°C~~, and a pressure range of 10 to 1200 hPa. It also provides GPS information, including time, longitude, latitude, and altitude.~~ ; humidity: 0-100 % RH). The whole procedure is programmable through a Micro Control Unit (MCU), and the sampling altitudes are pre-set before each flight.

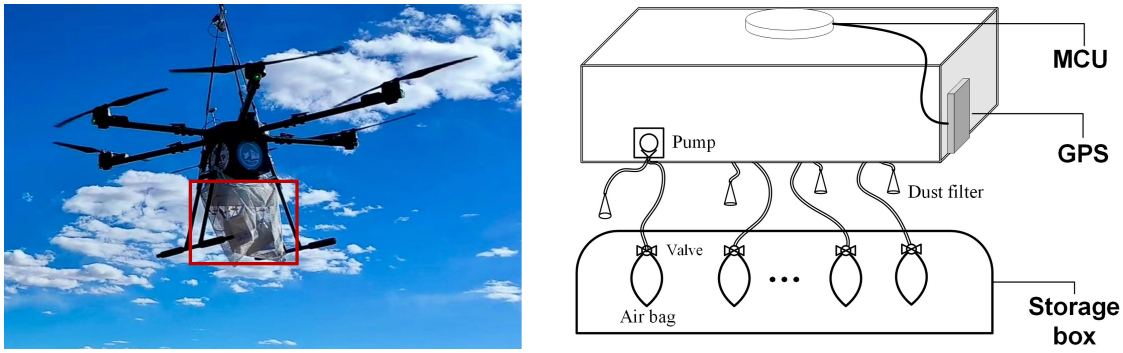

Figure 1. The design of the sampling system and its equipment on a UAV

2.2 Sampling procedure

The size of the gas collection system is $39\text{cm} \times 18\text{cm} \times 12\text{cm}$, and the total weight is 2.4 kg. The peak power of the sampling is about 10.8 W. An extra 12 V small Lithium battery (capacity of 2 Ah, and about 150 g weight) is used to power the pump. ~~Therefore, it~~ The whole system can be carried by UAVs with sufficient capacity. ~~small UAVs.~~ The following operations are performed before each flight: bags must be flushed with high-purity nitrogen at least 5 times before sampling; each bag must be carefully labelled to register its logging information, such as time, location and altitude for future analysis~~;~~ ~~concern~~ . Precautions must be taken when mounting sensors on UAV to prevent ~~pollution~~ contamination from human activities. The working flow chart ~~illustrated in~~ (Figure 2) provides a detailed view of the ~~process~~procedure, including pre-processing, parameter configuration, and operational ~~procedures~~steps.

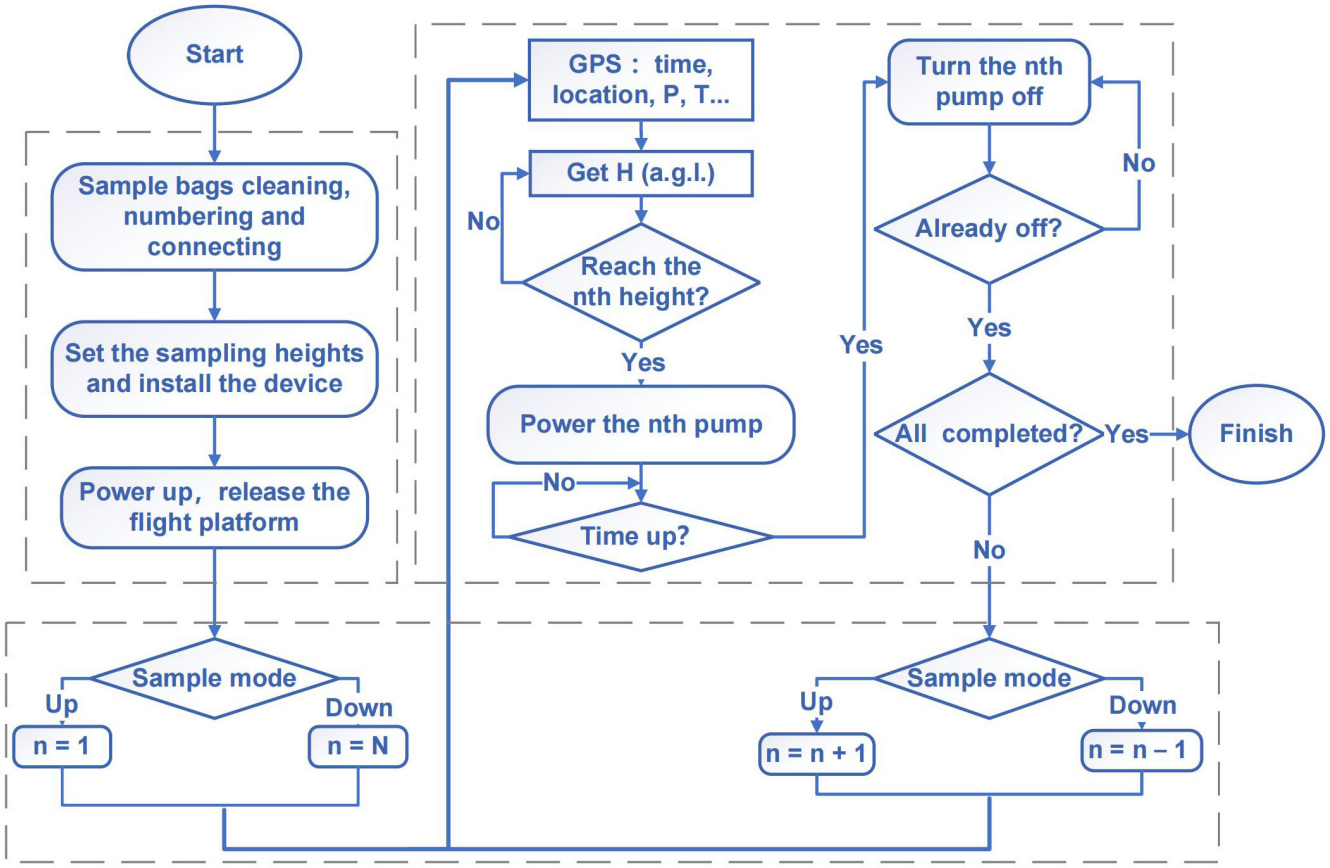

Figure 2. The working flowchart of the gas collection system

During the flights, the real-time altitude is calculated ~~on-line~~ at 1 Hz through pressure p and air temperature T collected from iMET XQ2 by:

$$Z = -\int_{p_0}^{p} \frac{RT}{g} d\ln p \tag{1}$$

where p_0 is the surface pressure, R is the ideal gas constant $287.05\mathrm{J}\cdot(\mathrm{kg}\cdot\mathrm{K})^{-1}$, g is the gravitational acceleration as a constant $9.80665\mathrm{m}\cdot\mathrm{s}^{-2}$. ~~While it is also feasible to use the UAV 's barometric and GPS-filtered altitude, we used the iMET XQ2 sensors to ensure consistency with the other atmospheric parameters being recorded and processed simultaneously.~~ Note that temperature and humidity data were not utilized for atmospheric boundary layer analysis due to potential interference from UAV heat sources and unshielded solar radiation, but they do not significantly affect altitude computations. A comparison of altitudes obtained from the iMET XQ2-based calculations with GPS measurements (as shown in Figure S1) indicates that

given the short flight durations (less than 40 minutes), the differences are negligible, remaining within 7 meters. This is minimal compared to the vertical sampling resolution of approximately 100 meters.

~~Due to the~~ The mobility and flexibility of the UAV platform (Figure 1) ~~, it can be used as a self-operating instrument for vertical distribution observation~~ make it an ideal autonomous system for vertical profile measurements of greenhouse gases. The sampling system ~~supports two modes of operation—Upand Down. Up mode: the UAV ascends quickly at an average speed of approximately~~ operates in two distinct modes: the ascent (Up) and descent (Down) modes.

In the Up mode, the UAV is operated with a relatively constant velocity of about 4 m/s ~~to a pre-set~~ until it reaches the predefined maximum altitude (~~e.g.,~~ for example, about 1300 m above ground level). ~~Due to energy efficiency considerations (Reuder et al., 2016), users need to hover~~ The samplings are collected during the ascent period. To optimize power consumption (Reuder et al., 2016), the system requires a stationary hovering phase at the target altitude to ~~allow the pump to function (as shown in~~ facilitate pump operation (as illustrated in the height stage pattern in Figure 3a). ~~The sampling motor runs for 11-20 seconds before stopping.Down mode: upon reaching the target altitude, the UAV hovers for about 10 seconds to collect the sample, after which the UAV automatically returns to its starting point with a slower descent~~

In the Down mode, the samples are collected during the descent period. The UAV initiates a 10-second hover at the maximum altitude for pump operation, followed by a gradual descent to the launch point (Figure 3b). ~~We recommend Down mode as it requires less manual operation, conserves energy, and reduces extra sampling time. Our study collected only~~

During the preliminary field campaign, we collected 15 samples ~~(in the first two flights) during the ascent phase. The operator manually controlled the loiter heights (as depicted in the height stage pattern in~~ exclusively with the Up mode in the two test flights. Maintaining UAV stability during manual altitude adjustments (Figure 3a) ~~, presenting a challenge for the UAV to maintain stability.~~ is the main challenge of the operation. Our experimental results demonstrate the superiority of the Down mode, which reduces manual intervention and enhances energy efficiency.

Each motor lasts 11-20 seconds and then stops. This sampling procedure repeats until the UAV lands on the ground, and the valves of airbags are closed. Above each valve, there is a sample cap with a silicone septum inside for syringe sampling.

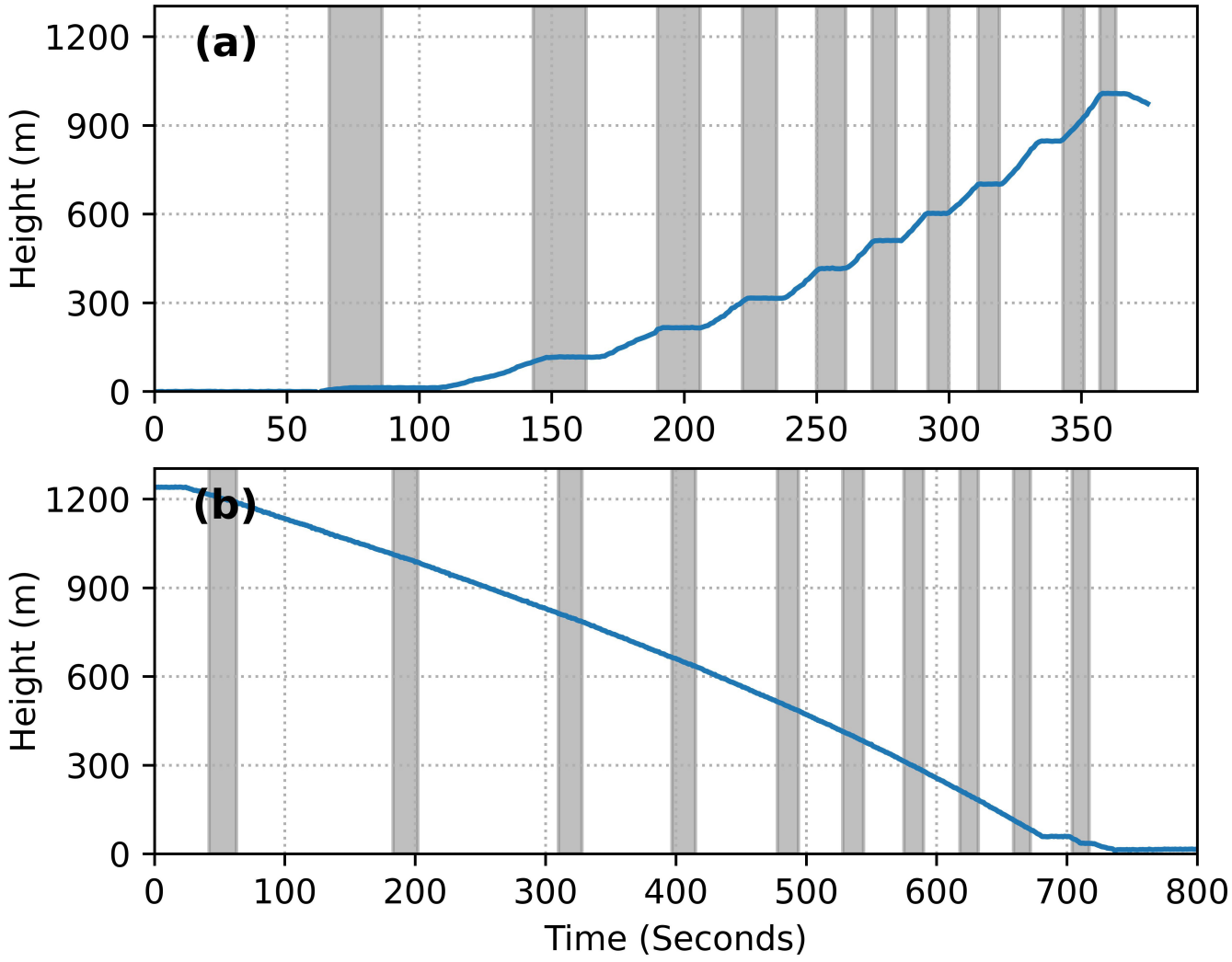

Figure 3. An example of sampling modes. The start times are (a) October 1 at 07:31, and (b) October 5 at 07:47(in local time). The lines indicate flight heights, while the gray shadows represent the operating times of each micro-motor.

2.3 Air sample analysis

The ~~collected bags are measured~~ air masses collected in the bags are analyzed with an Agilent GC 7890A (https://www.agilent.com.cn) ~~, and~~ for four GHG species (CO_2, CH_4, N_2O, SF_6)~~are simultaneously analyzed~~. The GC measurement is based on the ~~fact~~ principle that different components ~~mixed in the samples~~ within the sample flow at different speeds through the gas chromatography column, ~~therefore, different gases are perfectly separated and accurately measured~~enabling precise separation and accurate quantification of individual constituents. We use a 13X molecular sieve (13XMS) to separate CH_4 and a Porapak Q for

CO_2. Regarding N_2O and SF_6, they are separated from CO_2 by the Porapak Q column and then backflushed to the detector. The GC is equipped with a Flame Ionization Detector (FID) for detecting CH_4. CO_2 is converted to CH_4 using a nickel converter before being detected by the FID, as the FID only responds to carbon-containing organic compounds. Additionally, an Electron Capture Detector (ECD) is used for N_2O and SF_6. For ~~more~~ detailed information about the injector, gas line, valve-driving models, and laboratory accuracy testing, please refer to ~~the details in~~ our previous studies (Yuesi and Yinghong, 2003; Wang et al., 2010). The GC signals, mostly represented by ~~area or peak~~ peak area or height due to gas absorption, are directly ~~related and translated~~ proportional to gas concentrations~~, the~~ . These signals are carefully calibrated with standard gases ~~traced to the National Institute of Standards and Technology (NIST)~~ traceable to NIST scale. A linear regression is established between the peak area and the concentration of standard gases:

$$C = a \cdot \text{Area} + b \tag{2}$$

Where C represents the concentration of the detected gas, *Area* represents the peak area of the detected gas, and a and b are coefficients given through calibration with standard gas. The standard gas is injected multiple times (n≥7), and the standard deviation of parallel determinations is calculated to determine the detection limit and precision using a specific formula. Each type of GHG is measured in terms of its volume mixing ratio (VMR). The precisions, represented by the coefficients of variation, are 0.18 % for CO_2, 0.99 % for CH_4, 0.22 % for N_2O, and 1.7 % for SF_6 at the average levels of 0.75 ppm for CO_2, 0.02 ppm for CH_4, 0.74 ppb for N_2O, and 0.20 ppt for SF_6. The detection limits of this method are 2.4 ppm for CO_2, 0.07 ppm for CH_4, 2.6 ppb for N_2O and 1.5 ppt for SF_6.

3 Field Experiments

3.1 Sites

Field experiments were conducted at two high-altitude stations located in the Tibet Plateau:

(1) Cho Oyu basecamp (28.24°N, 86.59°E): This is a newly established temporary station ~~without~~ with no greenhouses measurements records ~~yet~~before. Its basecamp, located at 4,950 m a.s.l., serves as the starting point for the scientific research team to the summit of Mount Cho Oyu, which is about 8201 m a.s.l., the 6th highest mountain in the world.

(2) Qomolangma Station, CAS (28.36°N, 86.94°E): It is located at 4300 m a.s.l. and is on the northern slope of Mount Qomolangma (8848.86 m a.s.l., the highest mountain in the world). This station was established in 2005 by the Institute of Tibetan Plateau Research, Chinese Academy of Sciences (Ma et al., 2023).

Both sites are located in Tingri County, in Rikaze City, with detailed geographic location and elevation information provided in Figure 4.

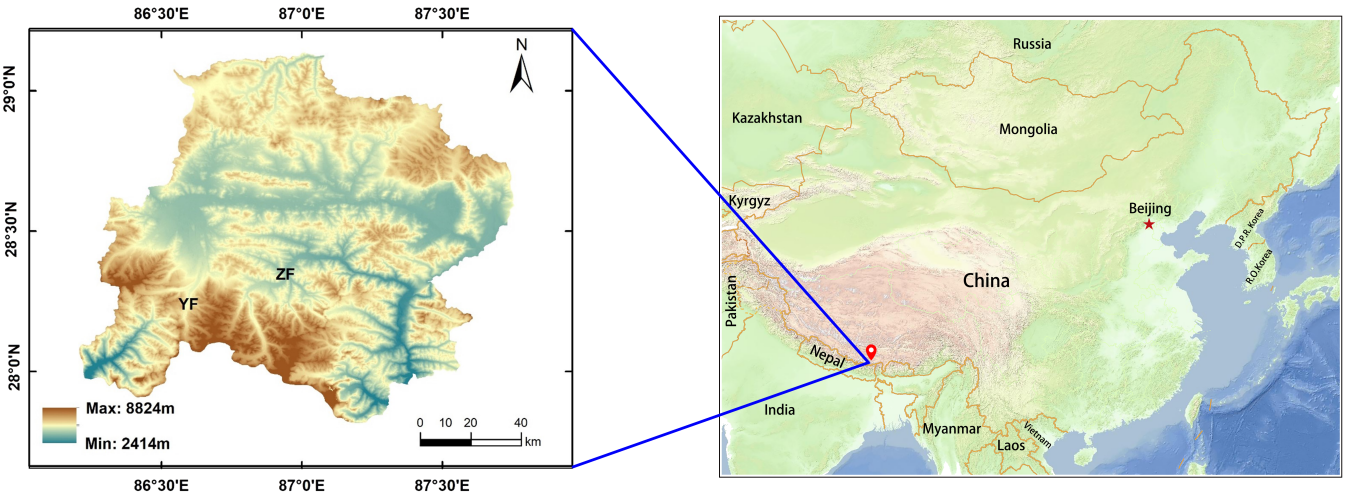

Figure 4. The ~~experiment~~ left panel shows the locations of the experimental sites, both situated in Tingri County: YF corresponds to the Cho Oyu base camp, and ZF corresponds to the Mount Qomolangma Station. The Digital Elevation Model (DEM) data is sourced from the Geospatial Data Cloud (http://www.gscloud.cn). The right panel shows the location of Tingri County on the map.

3.2 Results and analysis

Between 29 September and 03 October 2023, three flights were attempted in Cho Oyu, but only one flight succeeded due to bad weather conditions and MCU failures. On ~~Oct.03~~03 October, the system was transported to the Qomolangma Station ~~,~~ and 12 flights were successfully ~~operated in the next~~ conducted in the following 3 days.

During each flight, 10 bags were collected at 10 different altitudes, and it took about 40 minutes per flight. The flight and sampling information is listed in Table 1. In total, 139 samples were collected during the whole field campaign. The mean and standard deviation of the four greenhouse gases, as averaged across all samples, are listed in Table ~~2, showing low concentrations and minor variances.~~ 2.

Table 1. Sampling log of GHGs measurements during UAV flights in the Mount Qomolangma Region

Site	Local Date	Local Time	Max height(m)	Number of Samples
YF	2023/10/01	08:32	588.0	5
	2023/10/02	07:31	1007.9	10
	2023/10/03	11:53	1112.3	7
ZF	2023/10/03	15:35	1113.2	9
	2023/10/04	07:41	1113.8	10
		09:38	1214.9	10
		11:28	1213.2	10
		13:31	1212.9	10
		20:05	1214.4	9
	2023/10/05	07:42	1215.0	10
		09:47	1213.5	10
		11:37	1203.5	9
		13:43	1213.8	10
		16:34	1211.7	10
		20:36	1214.6	10

Table 2. Means and standard deviations of gas mixing ratios of all samples

Site	Time	CO_2 (ppm)	CH_4 (ppm)	N_2O (ppb)	SF_6 (ppt)
YF	2023/10/01-03	421.13±4.76	1.98±0.01	337.38±1.26	11.86±0.56
ZF	2023/10/03-05	418.35±2.54	2.00±0.02	337.15±1.41	11.76±0.54

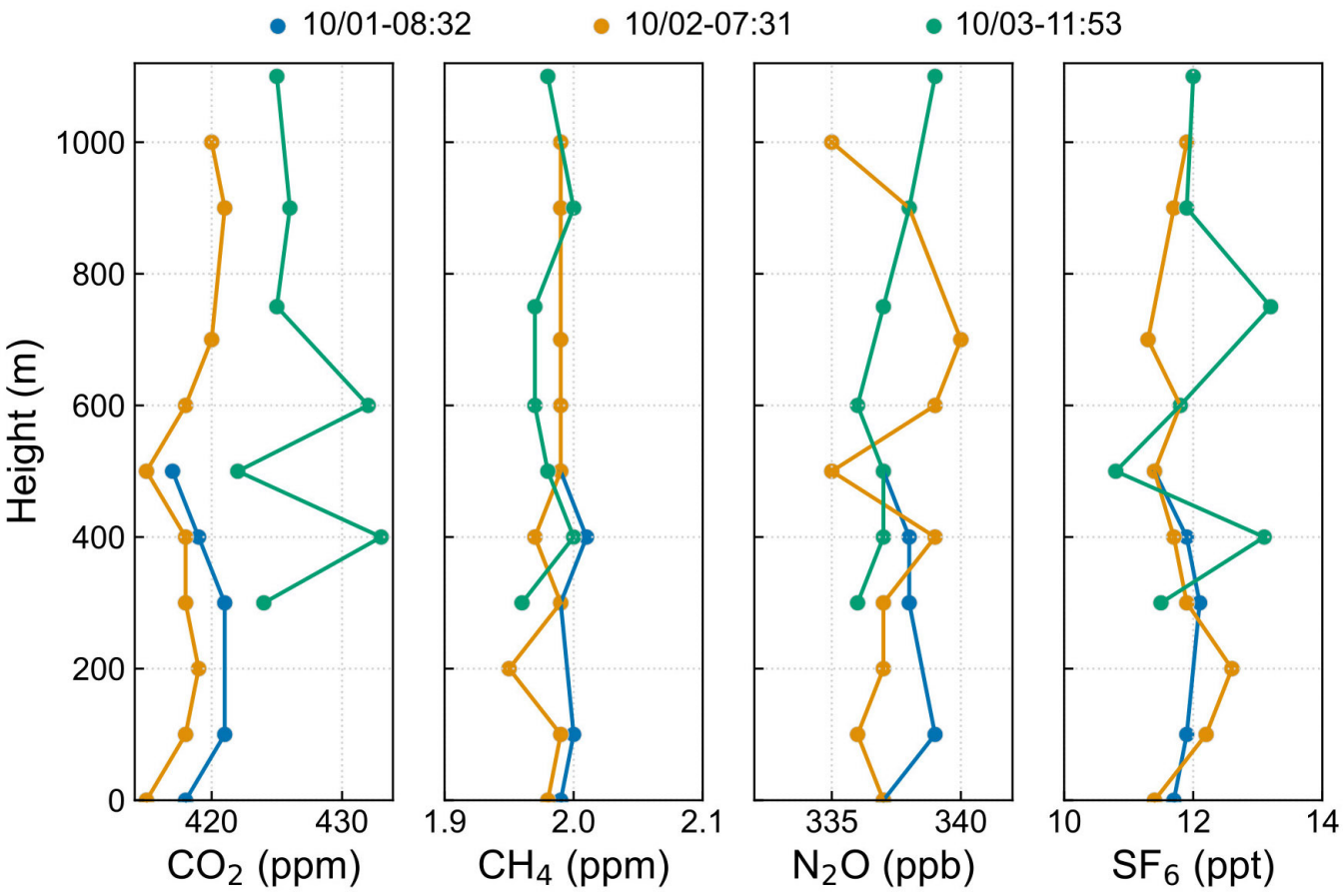

Figure 5. Profiles of 4 components (CO_2, CH_4, N_2O, SF_6) analyzed from Agilent GC 7890A and heights are measured by iMET XQ2 obtained in YF from 01 October to 03 October. The profiles in 01 October and 02 October are measured from ascent, and the profile in 03 October is from a descent.

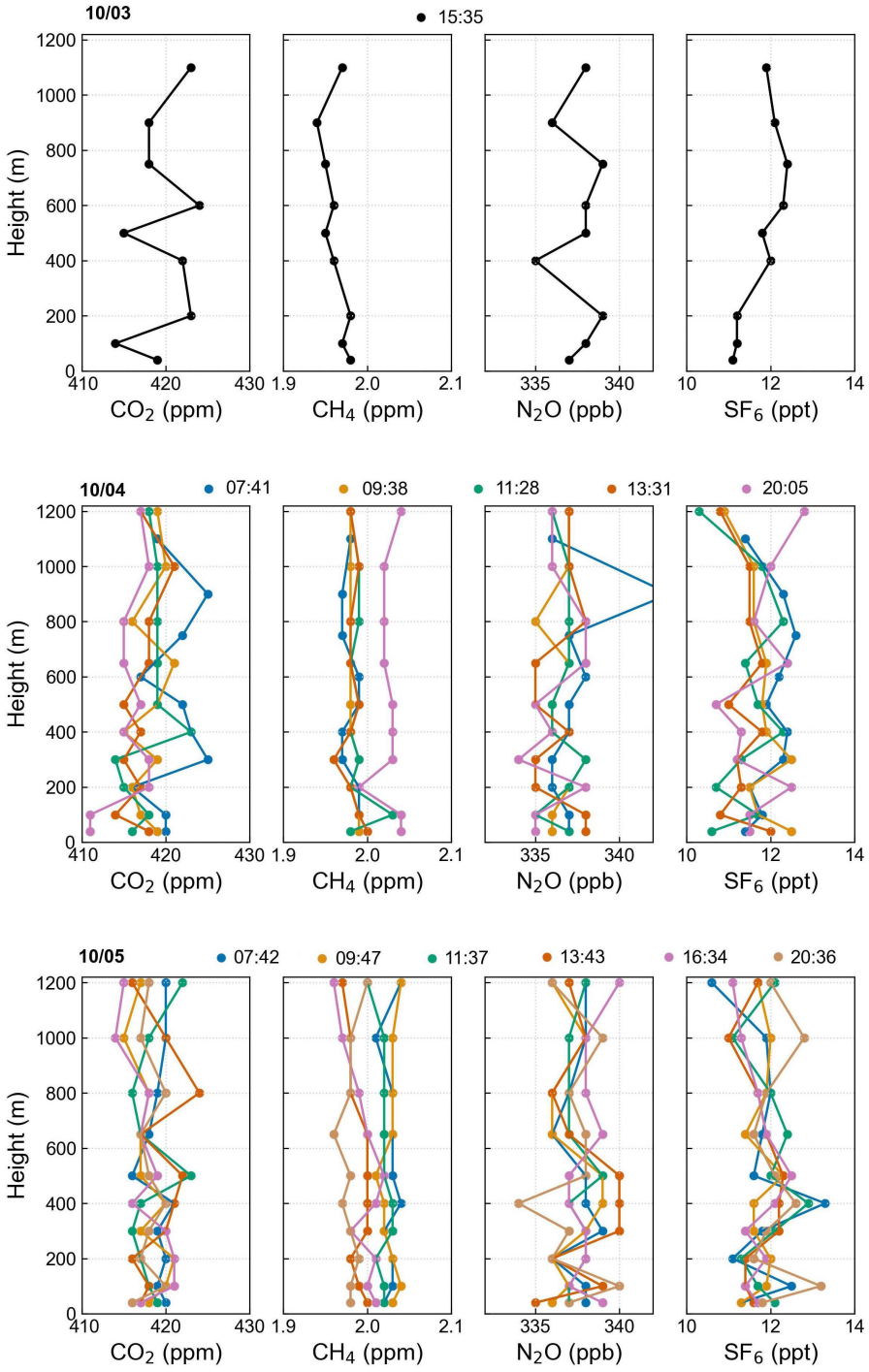

Figure 6. Same as Figure 5, but for ZF from 03 October to 05 October. The profiles are from descent.

~~The vertical distribution of four species is displayed in Figures~~ Figures 5 and 6 ~~for~~ show the vertical distribution of the four species at the Cho Oyu site and Qomolangma Station, respectively~~, showing irregular fluctuations~~. Small fluctuations along altitude are observed in CO_2, N_2O and SF_6 profiles, likely due to atmospheric turbulence, whereas CH_4 exhibit a more stable vertical distribution, ranging between 1.95 and 2.05 ppmv.

To examine the diurnal variation of GHGs, we compute the integral average of their mixing ratios. We also use ERA5 reanalysis data to determine the boundary layer height (BLH). This method allows us to categorize our samples into two distinct groups: those above the boundary layer and those below it. Figure 7 illustrates two time series of mixing ratios for four different species. The series for CO_2, N_2O, and SF_6 show a consistent pattern; however, the variations in CO_2 within the boundary layer height (BLH) are more pronounced than those above it. The downward trend observed on 04 October may reflect the intensification of natural processes due to sunlight and the increase in boundary layer height caused by solar heating. In contrast, CH_4 is well mixed; trends were inversely correlated with BLH and showed a slight increase on the night of 10/04 compared to the daytime. The increase in CH_4 levels exceeded the relative standard deviation (RSD) of our equipment, which may be attributed to local livestock or meadow emissions. ~~Due~~ Accurately quantifying and assessing the contributions of these factors remains challenging due to limited observational data and insufficient information on emission sources and meteorological conditions~~, accurately quantifying and assessing the contributions of these factors is challenging~~.

4 Conclusions

In this study, we developed a simple vertical stratified atmospheric sampling device that can be mounted on a middle-size UAV, a tethered balloon, or the roof of an electrical car, ~~which can get~~ enabling the collection of air samples at different altitudes or locations during a single flight ~~, either liftoff or return~~or cruise. After the collection is completed, the gas bag is closed to facilitate subsequent chromatography analysis to obtain the concentration of atmospheric components~~at multiple atmospheric altitudes~~. At the same time, the device ~~can record the~~ records the atmospheric temperature, pressure, humidity, and the location of each ~~layer of the atmosphere~~air sample.

~~In conclusion, the~~ The device has the following advantages: 1) its flexible design and adaptability make it suitable for integration with a variety of analytical instruments, enabling three-dimensional monitoring across diverse platforms; 2) its cost is less than US $ 5000, supporting widespread deployment and facilitating broader adoption in diverse research settings; 3) once the MCU is pre-set before the flight, its automatic operation and quick response time ensure simplicity and ease of use. As a result, this device is ~~suited~~ well-suited for extended periods of atmospheric observation and is minimally affected by terrain.

A 5-day continuous observation campaign was conducted at the Cho Oyu Base Camp and Qomolangma Station. We integrated the sampling system into a medium-sized hexacopter UAV platform and obtained 15 GHG vertical profiles up to 1215 m. ~~The temporal scope of the measurements, although informative, constrains the degree to which~~ While the temporal variations in GHG mixing ratios provide valuable insights, the limited number of data restricts the further analysis on how long-range transport ~~may have affected the observed trends~~processes and local sources and sinks may have influenced the observed variations. Greenhouse gases like CO_2 exhibit more pronounced variations within the boundary layer, while CH_4 levels rise slightly at night, potentially due to local emissions. This nocturnal increase in CH_4 could be linked to reduced atmospheric mixing during lower BLH, which leads to the accumulation of emissions near the surface. To enable continuous atmospheric monitoring (Kunz et al., 2018; Reuter et al., 2021), we still need to reduce equipment weight for easier long-term deployment. ~~It also helps us assess the distribution of greenhouse gases, elucidate~~ Extending these campaigns to long-term experiments at monthly to seasonal scales would enable the assessment of the GHG distribution, elucidation of their sources and sinks, and ~~disentangle~~ disentanglement of the signals from local vertical mixing ~~to~~ and long-range transport. It also has the potential to provide the prior value of vertical distributions of GHGs to calibrate and evaluate the satellite retrievals over complex topography~~. Comprehensive satellite observations (such as OCO-2, GOSAT, and Sentinel-5P) within a 100 km radius did not cover our region of the campaign. However, we have limited XCO_2 data from OCO-3 that aligns with our measurements. On 01 October 06:11 UTC, the XCO_2 values were 416.00 ppm at Qomolangma and 412.64 ppm at Cho Oyu. On 05 October 04:36 UTC, they were 417.96 ppm at Qomolangma and 414.66 ppm at Cho Oyu.~~, which are never measured before.

Although using UAVs or balloons to monitor or inspect GHG distributions at various sites has proven to be useful, this method has its limitations, including a relatively low sample resolution, as only 10 samples are collected. This results in a much coarser atmospheric profile, which is more challenging to relate to the atmospheric boundary layer ~~(ABL)~~ cycle. Additionally, the weight of the sampling device poses a challenge for smaller UAVs, making it less feasible for lightweight platforms. Adverse weather conditions such as strong winds, can interfere with the safe flight of these devices and the GPS

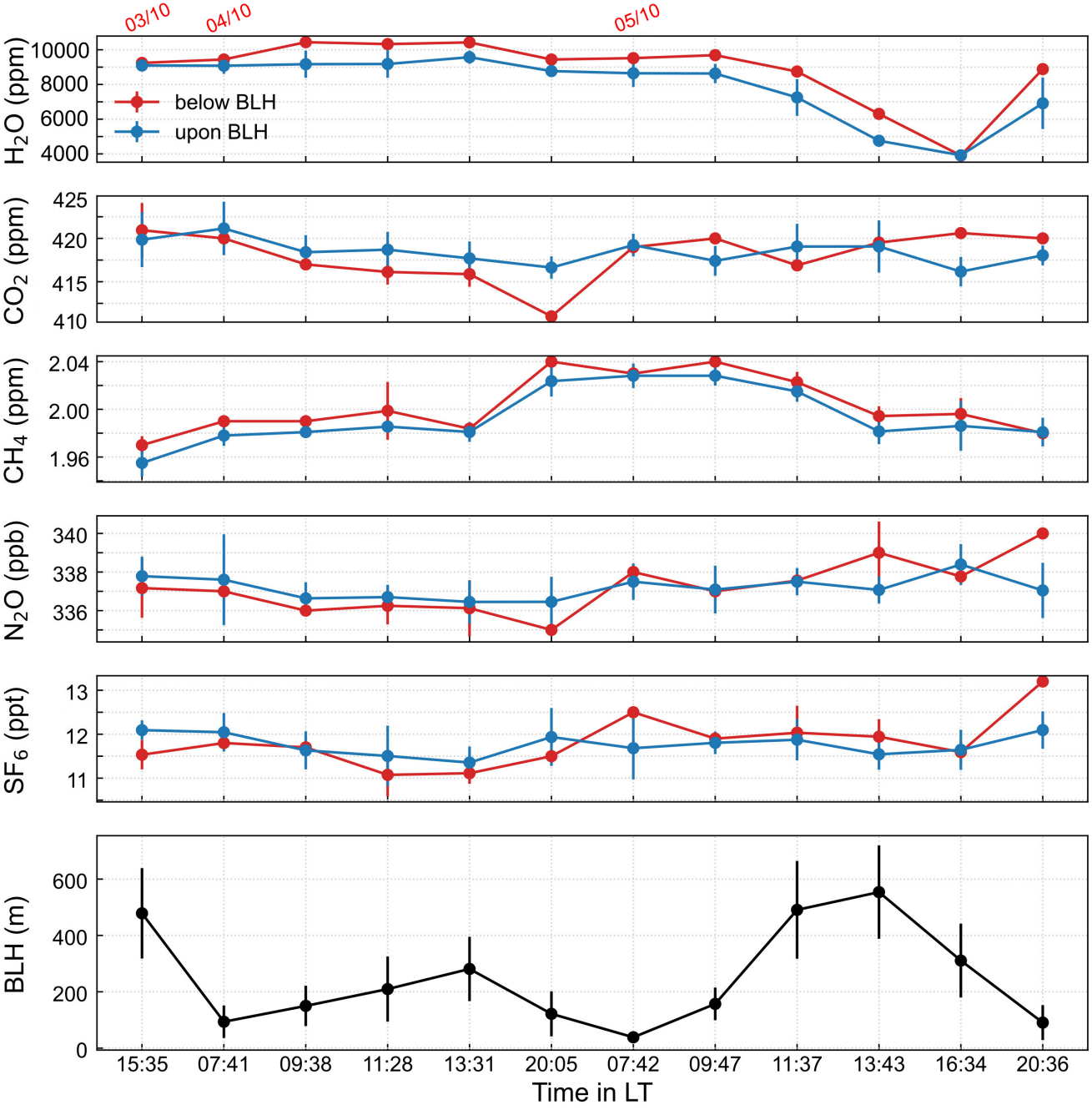

Figure 7. ~~Time~~ The time series ~~of~~ for 5 components (H_2O, CO_2, CH_4, N_2O, SF_6) ~~taken~~ in ZF from 03 October to 05 October~~and collocated boundary layer height data~~ , with mixing ratios using integrated average values, are displayed in the top 5 panels. BLH at the take-off location (28.36°N, 86.94°E) above ground level, sourced from ERA5 data, ~~utilizing~~ is displayed in the ~~integrated average value for each observation~~bottom panel. Error bars represent the ~~dispersion (~~standard deviation ~~)~~ of values across space.

signal. Furthermore, it is not advisable to use this technique for monitoring chemically active gas components in case the gas ~~content changes during transportation~~component may change after sampling. To address these issues, we will continue to optimize the design of the device to improve its performance and adaptability. We expect it to be used in a wider range of applications, such as understanding the sources and formation mechanisms of ~~air pollution events~~multiple gas tracers such as air pollutants.

Data availability. The observation data are available upon request from the corresponding author(dmz@mail.iap.ac.cn). ERA5 data used in this study are accessible from the ECMWF web page: https://www.ecmwf.int (last access: 6 October 2024; Hersbach et al. (2020)).

Author contributions. YZ, CQ, and MD contributed to the manufacturing of the sampling system. YW, MD, MZ, CQ, and YZ designed and conducted the campaign. YW, YZ, and CQ carried out the laboratory analyses, and YZ, MZ, MD, YW, and XT contributed to the preparation of the manuscript.

Competing interests. The authors declare no conflicts of interest.

Acknowledgements. This work was supported by the National Natural Science Foundation of China (42030107), and the Second Tibetan Plateau Scientific Expedition and Research Program (2022QZKK0101)

References

Bao, Z., Han, P., Zeng, N., Liu, D., Cai, Q., Wang, Y., Tang, G., Zheng, K., and Yao, B.: Observation and modeling of vertical carbon dioxide distribution in a heavily polluted suburban environment, Atmospheric and Oceanic Science Letters, 13, 371–379, 2020.

Britto Hupsel de Azevedo, G., Doyle, B., Fiebrich, C. A., and Schvartzman, D.: Low-complexity methods to mitigate the impact of environmental variables on low-cost UAS-based atmospheric carbon dioxide measurements, Atmospheric Measurement Techniques, 15, 5599–5618, 2022.

Brosy, C., Krampf, K., Zeeman, M., Wolf, B., Junkermann, W., Schäfer, K., Emeis, S., and Kunstmann, H.: Simultaneous multicopter-based air sampling and sensing of meteorological variables, Atmospheric Measurement Techniques, 10, 2773–2784, https://doi.org/10.5194/amt-10-2773-2017, 2017.

Buchwitz, M., de Beek, R., Noël, S., Burrows, J. P., Bovensmann, H., Bremer, H., Bergamaschi, P., Körner, S., and Heimann, M.: Carbon monoxide, methane and carbon dioxide columns retrieved from SCIAMACHY by WFM-DOAS: year 2003 initial data set, Atmospheric Chemistry and Physics, 5, 3313–3329, https://doi.org/10.5194/acp-5-3313-2005, 2005.

Byrne, B., Liu, J., Lee, M., Baker, I., Bowman, K. W., Deutscher, N. M., Feist, D. G., Griffith, D. W. T., Iraci, L. T., Kiel, M., Kimball, J. S., Miller, C. E., Morino, I., Parazoo, N. C., Petri, C., Roehl, C. M., Sha, M. K., Strong, K., Velazco, V. A., Wennberg, P. O., and Wunch, D.: Improved Constraints on Northern Extratropical CO2 Fluxes Obtained by Combining Surface-Based and Space-Based Atmospheric CO2 Measurements, Journal of Geophysical Research: Atmospheres, 125, e2019JD032 029, https://doi.org/https://doi.org/10.1029/2019JD032029, e2019JD032029 10.1029/2019JD032029, 2020.

Carnell, R. and Senior, C.: Changes in mid-latitude variability due to increasing greenhouse gases and sulphate aerosols, Climate Dynamics, 14, 369–383, 1998.

Chang, C.-C., Chang, C.-Y., Wang, J.-L., Pan, X.-X., Chen, Y.-C., and Ho, Y.-J.: An optimized multicopter UAV sounding technique (MUST) for probing comprehensive atmospheric variables, Chemosphere, 254, 126 867, https://doi.org/https://doi.org/10.1016/j.chemosphere.2020.126867, 2020.

Chevallier, F., Remaud, M., O'Dell, C. W., Baker, D., Peylin, P., and Cozic, A.: Objective evaluation of surface- and satellite-driven carbon dioxide atmospheric inversions, Atmospheric Chemistry and Physics, 19, 14 233–14 251, https://doi.org/10.5194/acp-19-14233-2019, 2019.

Etts, D., Rossi, M., Nzaou, R., Zhu, R., Lewin, G. C., and de Wekker, S. F.: Development of an autonomous multi-rotor copter for collecting atmospheric data near the ground, in: 2015 Systems and Information Engineering Design Symposium, pp. 120–124, https://doi.org/10.1109/SIEDS.2015.7116958, 2015.

Friedlingstein, P., O'sullivan, M., Jones, M. W., Andrew, R. M., Gregor, L., Hauck, J., Le Quéré, C., Luijkx, I. T., Olsen, A., Peters, G. P., et al.: Global carbon budget 2022, Earth System Science Data, 14, 4811–4900, https://doi.org/10.5194/essd-14-4811-2022, 2022.

Friedlingstein, P., O'sullivan, M., Jones, M. W., Andrew, R. M., Bakker, D. C., Hauck, J., Landschützer, P., Le Quéré, C., Luijkx, I. T., Peters, G. P., et al.: Global carbon budget 2023, Earth System Science Data, 15, 5301–5369, 2023.

Glaser, K., Vogt, U., Baumbach, G., Volz-Thomas, A., and Geiss, H.: Vertical profiles of O3, NO2, NOx, VOC, and meteorological parameters during the Berlin Ozone Experiment (BERLIOZ) campaign, Journal of Geophysical Research: Atmospheres, 108, https://doi.org/https://doi.org/10.1029/2002JD002475, 2003.

Han, T., Xie, C., Liu, Y., Yang, Y., Zhang, Y., Huang, Y., Gao, X., Zhang, X., Bao, F., and Li, S.-M.: Development of a continuous UAV-mounted air sampler and application to the quantification of CO 2 and CH 4 emissions from a major coking plant, Atmospheric Measurement Techniques, 17, 677–691, 2024.

Haszpra, L., Ramonet, M., Schmidt, M., Barcza, Z., Pátkai, Z., Tarczay, K., Yver, C., Tarniewicz, J., and Ciais, P.: Variation of CO_2 mole fraction in the lower free troposphere, in the boundary layer and at the surface, Atmospheric Chemistry and Physics, 12, 8865–8875, https://doi.org/10.5194/acp-12-8865-2012, 2012.

Hersbach, H., Bell, B., Berrisford, P., Hirahara, S., Horányi, A., Muñoz-Sabater, J., Nicolas, J., Peubey, C., Radu, R., Schepers, D., et al.: The ERA5 global reanalysis, Quarterly Journal of the Royal Meteorological Society, 146, 1999–2049, 2020.

IPCC: Climate Change 2021: The Physical Science Basis. Contribution of Working Group I to the Sixth Assessment Report of the Intergovernmental Panel on Climate Change, vol. In Press, Cambridge University Press, Cambridge, United Kingdom and New York, NY, USA, https://doi.org/10.1017/9781009157896, 2021.

Jiang, F., Wang, H. W., Chen, J. M., Zhou, L. X., Ju, W. M., Ding, A. J., Liu, L. X., and Peters, W.: Nested atmospheric inversion for the terrestrial carbon sources and sinks in China, Biogeosciences, 10, 5311–5324, https://doi.org/10.5194/bg-10-5311-2013, 2013.

Jin, Z., Tian, X., Wang, Y., Zhang, H., Zhao, M., Wang, T., Ding, J., and Piao, S.: A global surface CO_2 flux dataset (2015–2022) inferred from OCO-2 retrievals using the GONGGA inversion system, Earth System Science Data, 16, 2857–2876, https://doi.org/10.5194/essd-16-2857-2024, 2024.

Kuma, P., McDonald, A. J., Morgenstern, O., Querel, R., Silber, I., and Flynn, C. J.: Ground-based lidar processing and simulator framework for comparing models and observations (ALCF 1.0), Geoscientific Model Development, 14, 43–72, https://doi.org/10.5194/gmd-14-43-2021, 2021.

Kunz, M., Lavric, J. V., Gerbig, C., Tans, P., Neff, D., Hummelgård, C., Martin, H., Rödjegård, H., Wrenger, B., and Heimann, M.: COCAP: a carbon dioxide analyser for small unmanned aircraft systems, Atmospheric Measurement Techniques, 11, 1833–1849, 2018.

Li, Y., Deng, J., Mu, C., Xing, Z., and Du, K.: Vertical distribution of CO2 in the atmospheric boundary layer: Characteristics and impact of meteorological variables, Atmospheric Environment, 91, https://doi.org/10.1016/j.atmosenv.2014.03.067, 2014.

Liu, Y., Paris, J.-D., Vrekoussis, M., Antoniou, P., Constantinides, C., Desservettaz, M., Keleshis, C., Laurent, O., Leonidou, A., Philippon, C., et al.: Improvements of a low-cost CO 2 commercial nondispersive near-infrared (NDIR) sensor for unmanned aerial vehicle (UAV) atmospheric mapping applications, Atmospheric Measurement Techniques, 15, 4431–4442, 2022.

Loftfield, N., Flessa, H., Augustin, J., and Beese, F.: Automated gas chromatographic system for rapid analysis of the atmospheric trace gases methane, carbon dioxide, and nitrous oxide, Journal of Environmental Quality, 26, 560–564, 1997.

Ma, Y., Xie, Z., Ma, W., Han, C., Sun, F., Sun, G., Liu, L., Lai, Y., Wang, B., Liu, X., Zhao, W., Ma, W., Wang, F., Sun, L., Ma, B., Han, Y., Wang, Z., and Xi, Z.: QOMS: A Comprehensive Observation Station for Climate Change Research on the Top of Earth, Bulletin of the American Meteorological Society, 104, E563 – E584, https://doi.org/10.1175/BAMS-D-22-0084.1, 2023.

Masson-Delmotte, V., Zhai, P., Pörtner, H.-O., Roberts, D., Skea, J., Shukla, P. R., Pirani, A., Moufouma-Okia, W., Péan, C., Pidcock, R., et al.: Global warming of 1.5 C, An IPCC Special Report on the impacts of global warming of, 1, 93–174, 2019.

Neumann, P. P. and Bartholmai, M.: Real-time wind estimation on a micro unmanned aerial vehicle using its inertial measurement unit, Sensors and Actuators A: Physical, 235, 300–310, https://doi.org/https://doi.org/10.1016/j.sna.2015.09.036, 2015.

Niwa, Y., Machida, T., Sawa, Y., Matsueda, H., Schuck, T. J., Brenninkmeijer, C. A. M., Imasu, R., and Satoh, M.: Imposing strong constraints on tropical terrestrial CO2 fluxes using passenger aircraft based measurements, Journal of Geophysical Research: Atmospheres, 117, https://doi.org/https://doi.org/10.1029/2012JD017474, 2012.

O'Dell, C. W., Connor, B., Bösch, H., O'Brien, D., Frankenberg, C., Castano, R., Christi, M., Eldering, D., Fisher, B., Gunson, M., McDuffie, J., Miller, C. E., Natraj, V., Oyafuso, F., Polonsky, I., Smyth, M., Taylor, T., Toon, G. C., Wennberg, P. O., and Wunch, D.: The ACOS CO_2 retrieval algorithm – Part 1: Description and validation against synthetic observations, Atmospheric Measurement Techniques, 5, 99–121, https://doi.org/10.5194/amt-5-99-2012, 2012.

Ramanathan, A., Nguyen, H. M., Sun, X., Mao, J., Abshire, J. B., Hobbs, J., and Braverman, A.: A singular value decomposition framework for retrievals with vertical distribution information from greenhouse gas column absorption spectroscopy measurements, Atmospheric Measurement Techniques, 11, 4909–4928, https://doi.org/https://doi.org/10.5194/AMT-11-4909-2018, 2018.

Ren, W., Tian, H., Xu, X., Liu, M., Lu, C., Chen, G., Melillo, J., Reilly, J., and Liu, J.: Spatial and temporal patterns of CO2 and CH4 fluxes in China's croplands in response to multifactor environmental changes, Tellus B: Chemical and Physical Meteorology, 63, 222–240, 2011.

Reuder, J., Båserud, L., Jonassen, M. O., Kral, S. T., and Müller, M.: Exploring the potential of the RPA system SUMO for multipurpose boundary-layer missions during the BLLAST campaign, Atmospheric Measurement Techniques, 9, 2675–2688, 2016.

Reuter, M., Bovensmann, H., Buchwitz, M., Borchardt, J., Krautwurst, S., Gerilowski, K., Lindauer, M., Kubistin, D., and Burrows, J. P.: Development of a small unmanned aircraft system to derive CO 2 emissions of anthropogenic point sources, Atmospheric Measurement Techniques, 14, 153–172, 2021.

Sun, X., Duan, M., Gao, Y., Han, R., Ji, D., Zhang, W., Chen, N., Xia, X., Liu, H., and Huo, Y.: In situ measurement of CO_2 and CH_4 from aircraft over northeast China and comparison with OCO-2 data, Atmospheric Measurement Techniques, 13, 3595–3607, https://doi.org/10.5194/amt-13-3595-2020, 2020.

Wang, Y., Wang, Y., and Ling, H.: A new carrier gas type for accurate measurement of N 2 O by GC-ECD, Advances in Atmospheric Sciences, 27, 1322–1330, https://doi.org/10.1007/s00376-010-9212-2, 2010.

Wheeler, M., Newman, S., Orr-Ewing, A., and Ashfold, M.: Cavity ring-down spectroscopy, J. Chem. Soc., Faraday Trans., 94, 337–351, https://doi.org/10.1039/A707686J, 1998.

Wilkinson, J., Bors, C., Burgis, F., Lorke, A., and Bodmer, P.: Measuring CO2 and CH4 with a portable gas analyzer: Closed-loop operation, optimization and assessment, PloS one, 13, e0193 973, https://doi.org/https://doi.org/10.1371/journal.pone.0193973, 2018.

Wunch, D., Toon, G. C., Blavier, J.-F. L., Washenfelder, R. A., Notholt, J., Connor, B. J., Griffith, D. W., Sherlock, V., and Wennberg, P. O.: The total carbon column observing network, Philosophical Transactions of the Royal Society A: Mathematical, Physical and Engineering Sciences, 369, 2087–2112, https://doi.org/10.1098/rsta.2010.0240, 2011.

Xie, S.-P., Lu, B., and Xiang, B.: Similar spatial patterns of climate responses to aerosol and greenhouse gas changes, Nature Geoscience, 6, 828–832, 2013.

Yoshida, Y., Kikuchi, N., Morino, I., Uchino, O., Oshchepkov, S., Bril, A., Saeki, T., Schutgens, N., Toon, G., Wunch, D., et al.: Improvement of the retrieval algorithm for GOSAT SWIR XCO 2 and XCH 4 and their validation using TCCON data, Atmospheric Measurement Techniques, 6, 1533–1547, https://doi.org/10.5194/amt-6-1533-2013, 2013.

Yuesi, W. and Yinghong, W.: Quick measurement of CH 4, CO 2 and N 2 O emissions from a short-plant ecosystem, Advances in Atmospheric Sciences, 20, 842–844, https://doi.org/10.1007/BF02915410, 2003.